J Mater Sci (2011) 46:1076–1082
DOI 10.1007/s10853-010-4875-8

Recrystallization behaviors of alloy IC10 at elevated temperature: experiments and modeling

Hongjian Zhang · Weidong Wen · Haitao Cui · Ying Xu

Received: 25 November 2009 / Accepted: 30 August 2010 / Published online: 9 September 2010

Abstract IC10 is a newly developed Ni_3Al-based superalloy. In order to investigate the recrystallization behaviors of IC10, tensile experiments were conducted over a wide range of strain rates (10^{-4}–$10^{-2}s^{-1}$) and temperatures (1173–1373 K) on a material testing system (MTS809). And the TEM examinations were operated to characterize deformation mechanisms of IC10. Experiments show that: (1) at the temperature range from 1173 to 1373 K, the domination behavior of IC10 is recrystallization behavior; (2) the flow stress depends to a high degree on the strain rates and temperatures; (3) there are both edge and screw dislocations on the cube plane, and these dislocations have a tendency to form the slipbands at the interphase boundaries, which is the domination mechanism of recrystallization behaviors. In order to capture the flow features of IC10, a new phenomenological constitutive equation is developed. The new model is used to describe the recrystallization behaviors of IC10 at various conditions. The predicted data fit well with the experiments, and the average relative errors at various conditions are less than 3%. It shows that the model is valid.

Introduction

Ordered Ni_3Al-based intermetallic compounds have the features of high specific modules, high yield strength, fairly good ductility from room temperature to elevated temperature, high incipient melting temperature, excellent oxidation resistance, and high creep resistance over a wide range of temperatures [1–3]. During the past few decades, such materials have been intensively studied as potential high temperature structural materials in the aerospace applications. As such materials exhibit anomalous thermo-mechanical properties, including the positive temperature dependence of the flow stress, the strain-hardening rate (SHR), a tension–compression asymmetry etc., there have been significant efforts to clarify the micro-mechanisms responsible for the anomalous features, and various mechanistic models have been proposed based upon this body of research. The most representative models include: TK model [4], PPV model [5], Superkink model [6], ELU model [7], Hirsch's model [8, 9], Yuan and Parks' model [10], Cuitiño and Ortiz's model [11], Choi's model [12, 13], etc. All these models are successful in describing the anomalous features of such materials. But to the authors' knowledge, there is no constitutive equation on the recrystallization behaviors of Ni_3Al-based alloys.

Generally speaking, the evolution of the microstructure under high temperatures involves strain hardening, dynamic recovery, recrystallization, and grain growth, all of which are highly temperature-dependent and rate-dependent. In particular, recrystallization leads to the local elimination of a large number of dislocations and is generally associated with a decrease in the average grain size. Although state-variable based constitutive equations for materials undergoing hot work are successful in describing strain hardening and dynamic recovery, the limited work has been done in addressing dynamic recrystallization within a continuum framework.

Alloy IC10 is a newly developed Ni_3Al-based superalloy, which is a kind of potential advanced aero-engine van materials with a service temperature up to 1373 K [14].

H. Zhang (✉) · W. Wen · H. Cui · Y. Xu
College of Energy and Power Engineering, Nanjing University of Aeronautics and Astronautics, 210016 Nanjing, Jiangsu, People's Republic of China
e-mail: zhanghongjian@nuaa.edu.cn; hongjian_zhang@hotmail.com

Extensive studies have been made to describe the hardening behaviors of alloy IC10 successfully [15–19]. But the studies about the recrystallization behaviors of alloy IC10 at elevated temperatures are still very rare. The objective of this article is to investigate the recrystallization behaviors of IC10 based on experiments and to develop a new constitutive model to describe the behaviors.

Experimental procedures

Experimental material

A Ni_3Al-based alloy IC10, supplied by the AVIC1 Beijing institute of aeronautical materials, is directional solidification material in [001] orientation, with its nominal composition(wt%): 0.07–0.12%C, 11.5–12.5%Co, 6.5–7.5%Cr, 5.6–6.2%Al, 4.8–5.2%W, 1.0–2.0%Mo, 6.5–7.5%Ta, 1.3–1.7%Hf, 0.01–0.02%B, and Bal. Ni. The master alloy ingot of IC10 was first prepared by a vacuum induction furnace. Then the master alloy ingot was cut to several smaller ingots with its weight of 4 kg. And the smaller ingots were processed to directional solidification bars of ∅15 mm in [001] orientation in directional solidification vacuum induction furnace. Then, the as-cast bars were heat-treated as the following processes: (1) homogenized at 1453 K for 2 h, and increased the temperature to 1543 K to homogenize for 2 h, followed by air-cooling to room temperature; (2) increased the temperature to 1323 K to homogenize for 4 h, and air-cooling to room temperature; (3) increased temperature to 1143 K to homogenize for 16 h, followed by air-cooling. The columnar tensile specimens with dimension of ϕ 10 × 50 mm^2 were machined from the bars.

Figure 1 shows the typical microstructures of alloy IC10. As seen in a SEM micrograph in Fig. 1a, there are some unsolutioned γ/γ' eutectic and resolved MC. This is because that the initial melting temperature of γ' is lower than its total melting temperature caused by the existence of the trace elements, such as B, Hf, C, etc. As seen in Fig. 1b, the size of γ' particles ranges from 0.2 to 0.6 μm. By image analysis, the volume fraction of γ' phase was found to be about 65%.

Test equipment and procedures

In order to investigate recrystallizational behaviors of IC10, tensile experiments were carried out over a wide range of temperatures (1173–1373 K) and strain rates (10^{-4}–$10^{-2}s^{-1}$). The experimental temperature is attained with a high-intensity quartz lamp, in a radiant-heating furnace (MTS653 furnace). All the tests were conducted on Material Test System (MTS809), a computer-controlled,

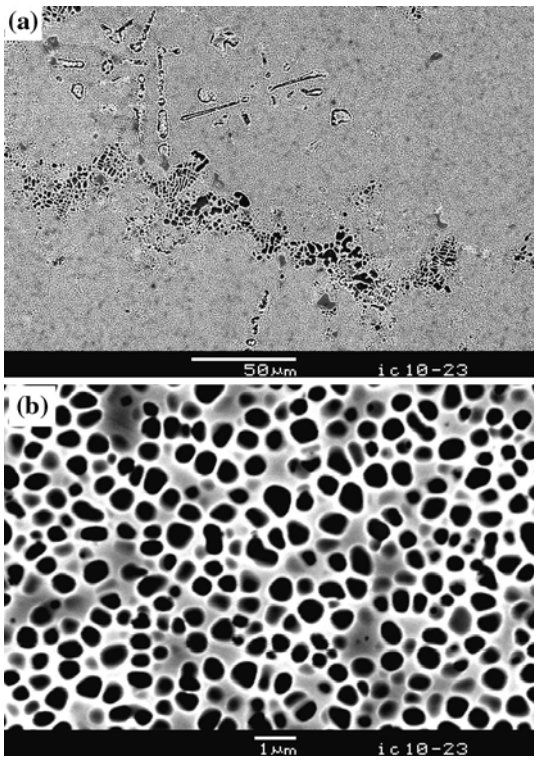

Fig. 1 Typical microstructures of alloy IC10 after heat treatment **a** morphology of unsolutioned γ/γ' eutectic and resolved MC, and **b** spherical γ' phase

servo-hydraulic tensile torsion machine. All the specimens were deformed to fracture and then air cooled to room temperature. The experimental data were gathered at the velocity of 10/s by the signal automatism gather system of MTS809.

In order to characterize deformation mechanisms of IC10, the TEM examinations were operated. For TEM examinations, slices parallel and vertical to the tensile axis were cut from some specimens by spark erosion. The foils were prepared using twin-jet electropolishing and were examined on a JEM-2010 analytical transmission electron microscope.

Experimental results and discussion

Figure 2 shows the stress–strain curves of alloy IC10 over the range of the strain rates from 10^{-4} to $10^{-2}s^{-1}$ and temperatures from 1173 to 1373 K. The stress–strain curves in Fig. 2 show that: (1) the flow stress initially increases positively with the strain before the critical strain, and then the softening happens after the critical strain, which is the typical dynamic recrystallization curve; (2) the flow stress depends to a high degree on the strain rate, and its value increases obviously with strain rate; (3) the flow stress is also sensitive to temperature. With the increase of

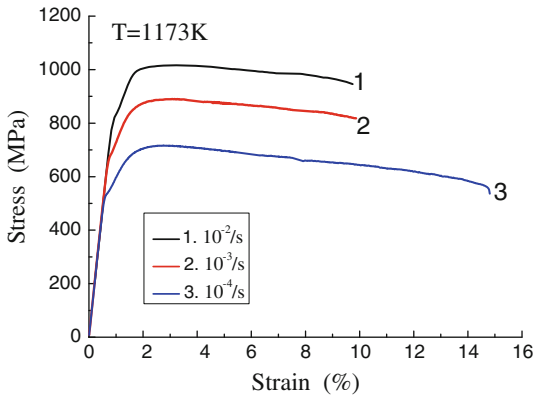

(a) T=1173K

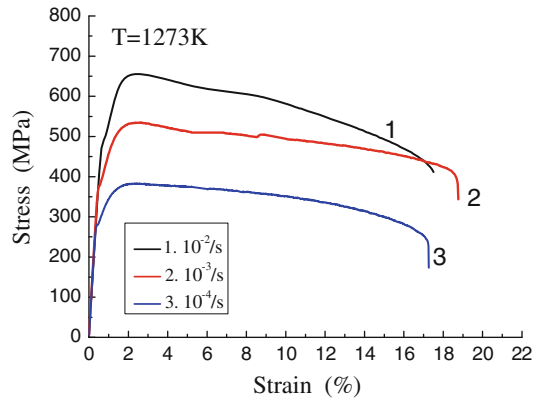

(b) T=1273K

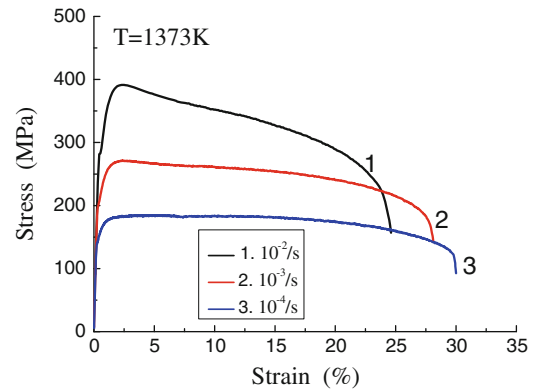

(c) T=1373K

Fig. 2 $\sigma - \varepsilon$ curves of IC10 at different strain rates and temperatures

temperature, the critical strain reduces and the value of flow stress decreases at the rate of 30–40%/100 K.

Figure 3 shows the bright-field images of dislocation structures in foils from specimens deformed to fracture with different strain rate at 1173 K. As shown on Fig. 3, the dislocation density in γ phase is larger than in γ' phase. And the dislocations have a tendency to form either edge or screw segments on the cube plane so that almost regular square nets of dislocations can be observed. The geometry of the nets suggests that the respective mobility of screw and edge segments is comparable.

A great number of dislocation nets will lead to the formation of the slipbands at the interphase boundaries. During the formation process, a lot of dislocations are annihilated leading to the decrease of dislocation density and the softening effect of material. It is well-known that the dislocation will multiply greatly in the process of deformation. And the multiplication will lead to the hardening effect of material. At the beginning of deformation, the multiplication rate is greater than the annihilation rate, and the hardening effect dominates. When the dislocation density achieves a critical value, the multiplication rate is equal to the annihilation rate, and flow stress gets saturation. After that, the softening effect will dominate if the multiplication rate is less than the annihilation rate. That is the mechanism of recrystallization behavior of metals.

Constitutive equation of recrystallization behaviors

Development of new constitutive equation

A new constitutive equation is proposed for describing the recrystallization behaviors as following formulations:

$$\sigma = \sigma_c - K(\Delta\varepsilon)^n = \begin{cases} \sigma_c - K_h(\varepsilon_c - \varepsilon)^{n_h} & \varepsilon \le \varepsilon_c \\ \sigma_c - K_s(\varepsilon - \varepsilon_c)^{n_s} & \varepsilon > \varepsilon_c \end{cases} \quad (1)$$

where, σ is the stress, $K(K_h, K_s)$ and $n(n_h, n_s)$ are parameters. The subscripts (h and s) refer to strain hardening part before the critical strain ε_c, and softening part after the critical strain ε_c, respectively. σ_c is the critical stress at the strain of ε_c. $\Delta\varepsilon$ is equal to $|\varepsilon_c - \varepsilon|$.

As seen from Eq. 1, the formulation $\sigma = \sigma_c - K_h(\varepsilon_c - \varepsilon)^{n_h}$ is used to describe the strain hardening part, and the equation $\sigma = \sigma_c - K_s(\varepsilon - \varepsilon_c)^{n_s}$ is for the softening part.

Normally, the feature of the stress–strain curve is determined by the parameters K and n, which are assumed to be constants at a decided experimental condition and vary with the mechanical properties, such as yield stress $\sigma_{0.2}$, the critical stress/strain (σ_c/ε_c), fracture stress σ_b, and elongationε_b. The variation rules will be discussed in the following section.

Based on Eq. 1, the relationship between the stress and plastic strain of a random point P in the curve follows that,

$$\sigma_P = \sigma_c - K(\Delta\varepsilon_P)^n \quad (2)$$

where, σ_P is the stress of P, $\Delta\varepsilon_P = |\varepsilon_c - \varepsilon_P^p|$, ε_P^p is the plastic strain of P.

When the point P is the yield point, we obtain:

$$\sigma_{0.2} = \sigma_c - K_h(\Delta\varepsilon_{0.2})^{n_h} = \sigma_c - K_h(\varepsilon_c - \varepsilon_{0.2})^{n_h} \quad (3)$$

From Eq. 3, we can get the formulation of K_h:

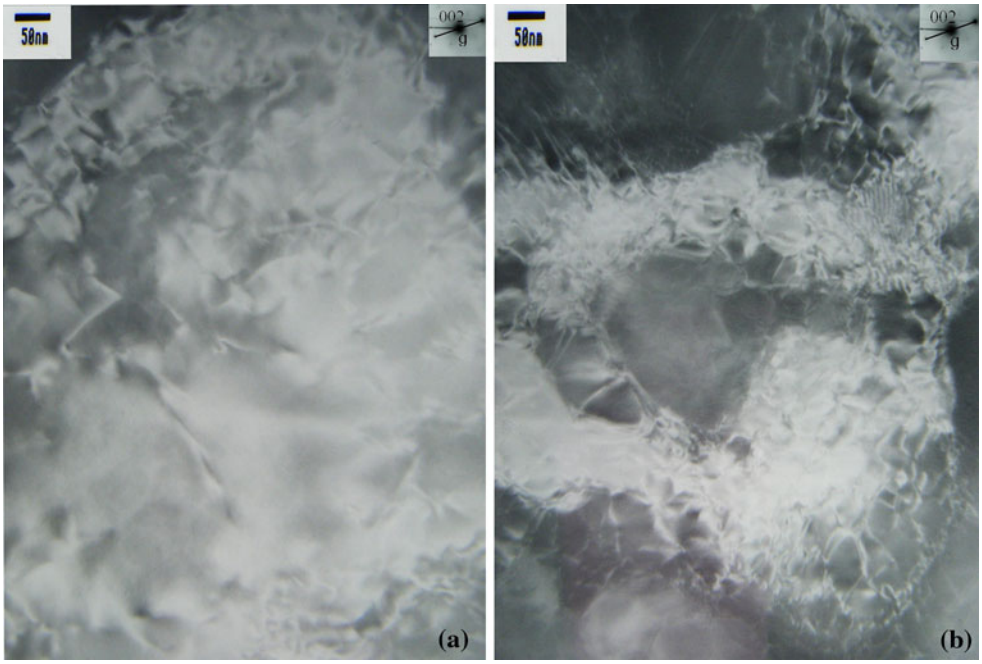

Fig. 3 The bright-field images of dislocation structures after deformed to fracture at 1173 K. **a** $T = 1173$ K, $\dot{\varepsilon} = 10^{-3}/\mathrm{s}$ and **b** $T = 1173$ K, $\dot{\varepsilon} = 10^{-4}/\mathrm{s}$

$$K_{\mathrm{h}} = \frac{(\sigma_{\mathrm{c}} - \sigma_{0.2})}{(\Delta\varepsilon_{0.2})^{n}} \tag{4}$$

When the point P is the fracture point, we obtain:

$$\sigma_{\mathrm{b}} = \sigma_{\mathrm{c}} - K_{\mathrm{s}}(\Delta\varepsilon_{\mathrm{b}})^{n_{\mathrm{s}}} = \sigma_{\mathrm{c}} - K_{\mathrm{s}}(\varepsilon_{\mathrm{b}} - \varepsilon_{\mathrm{c}})^{n_{\mathrm{s}}} \tag{5}$$

From Eq. 5, we can get the formulation of K_{s}:

$$K_{\mathrm{s}} = \frac{(\sigma_{\mathrm{c}} - \sigma_{\mathrm{b}})}{(\Delta\varepsilon_{\mathrm{b}})^{n}} \tag{6}$$

When the point P locates at the hardening part, we can get the following equation from Eqs. 2 and 3.

$$\frac{\sigma_{\mathrm{c}} - \sigma_{0.2}}{\sigma_{\mathrm{c}} - \sigma_{P}} = \left(\frac{\Delta\varepsilon_{0.2}}{\Delta\varepsilon_{P}}\right)^{n_{\mathrm{h}}} \tag{7}$$

Using Log function on both sides of Eq. 7, we can get:

$$\begin{aligned} n_{\mathrm{h}} &= \frac{\ln((\sigma_{\mathrm{c}} - \sigma_{0.2})/(\sigma_{\mathrm{c}} - \sigma_{P}))}{\ln(\Delta\varepsilon_{0.2}/\Delta\varepsilon_{P})} \\ &= \frac{\ln(\sigma_{\mathrm{c}} - \sigma_{0.2}) - \ln(\sigma_{\mathrm{c}} - \sigma_{P})}{\ln(\Delta\varepsilon_{0.2}) - \ln(\Delta\varepsilon_{P})} \end{aligned} \tag{8}$$

As $(\sigma_{\mathrm{c}} - \sigma_{P})$ is less than $(\sigma_{\mathrm{c}} - \sigma_{0.2})$, and ln $(\Delta\varepsilon_{P})$ is less than ln $(\Delta\varepsilon_{0.2})$, we assume that:

$$\ln(\sigma_{\mathrm{c}} - \sigma_{P}) = a_1 \ln(\sigma_{\mathrm{c}} - \sigma_{0.2}) \tag{9}$$

$$\ln(\Delta\varepsilon_{P}) = b_1 \ln(\Delta\varepsilon_{0.2}) \tag{10}$$

where the parameters a_1 and b_1 are the constants in the range of (0–1).

Considering the Eqs. 8–10 together, we obtain:

$$n_{\mathrm{h}} = \frac{(1 - a_1)\ln(\sigma_{\mathrm{c}} - \sigma_{0.2})}{(1 - b_1)\ln(\Delta\varepsilon_{0.2})} \tag{11}$$

When the point P locates at the softening part, we can get the following equation from Eqs. 2 and 5.

$$\frac{\sigma_{\mathrm{c}} - \sigma_{\mathrm{b}}}{\sigma_{\mathrm{c}} - \sigma_{P}} = \left(\frac{\Delta\varepsilon_{\mathrm{b}}}{\Delta\varepsilon_{P}}\right)^{n_{\mathrm{s}}} \tag{12}$$

Using Log function on both sides of Eq. 12, we can get:

$$\begin{aligned} n_{\mathrm{s}} &= \frac{\ln((\sigma_{\mathrm{c}} - \sigma_{\mathrm{b}})/(\sigma_{\mathrm{c}} - \sigma_{P}))}{\ln(\Delta\varepsilon_{\mathrm{b}}/\Delta\varepsilon_{P})} \\ &= \frac{\ln(\sigma_{\mathrm{c}} - \sigma_{\mathrm{b}}) - \ln(\sigma_{\mathrm{c}} - \sigma_{P})}{\ln(\Delta\varepsilon_{\mathrm{b}}) - \ln(\Delta\varepsilon_{P})} \end{aligned} \tag{13}$$

As $(\sigma_{\mathrm{c}} - \sigma_{P})$ is less than $(\sigma_{\mathrm{c}} - \sigma_{\mathrm{b}})$, and ln $(\Delta\varepsilon_{P})$ is less than ln $(\Delta\varepsilon_{b})$, we assume:

$$\ln(\sigma_{\mathrm{c}} - \sigma_{P}) = a_2 \ln(\sigma_{\mathrm{c}} - \sigma_{\mathrm{b}}) \tag{14}$$

$$\ln(\Delta\varepsilon_{P}) = b_2 \ln(\Delta\varepsilon_{\mathrm{b}}) \tag{15}$$

where the parameters a_2 and b_2 are the constants in the range of (0–1).

Considering the Eqs. 13–15 together, we get:

$$n_{\mathrm{s}} = \frac{(1 - a_2)\ln(\sigma_{\mathrm{c}} - \sigma_{\mathrm{b}})}{(1 - b_2)\ln(\Delta\varepsilon_{\mathrm{b}})} \tag{16}$$

As the parameters n_{h} and n_{s} are assumed to be constants at a decided experimental condition, the relationships of n_{h}, n_{s} between different conditions can be derived from Eqs. 11 and 16:

$$\frac{n_{\mathrm{hN}}}{n_{h\mathrm{R}}}=\frac{\frac{(1-a_{1\mathrm{N}})}{(1-b_{1\mathrm{N}})}\left(\frac{\ln(\sigma_{\mathrm{c}}-\sigma_{0.2})}{\ln(\Delta\varepsilon_{0.2})}\right)_{\mathrm{N}}}{\frac{(1-a_{1\mathrm{R}})}{(1-b_{1\mathrm{R}})}\left(\frac{\ln(\sigma_{\mathrm{c}}-\sigma_{0.2})}{\ln(\Delta\varepsilon_{0.2})}\right)_{\mathrm{R}}}\approx\frac{\left(\frac{\ln(\sigma_{\mathrm{c}}-\sigma_{0.2})}{\ln(\Delta\varepsilon_{0.2})}\right)_{\mathrm{N}}}{\left(\frac{\ln(\sigma_{\mathrm{c}}-\sigma_{0.2})}{\ln(\Delta\varepsilon_{0.2})}\right)_{\mathrm{R}}} \tag{17}$$

$$\frac{n_{\mathrm{sN}}}{n_{\mathrm{sR}}}=\frac{\frac{(1-a_{2\mathrm{N}})}{(1-b_{2\mathrm{N}})}\left(\frac{\ln(\sigma_{\mathrm{c}}-\sigma_{\mathrm{b}})}{\ln(\Delta\varepsilon_{\mathrm{b}})}\right)_{\mathrm{N}}}{\frac{(1-a_{2\mathrm{R}})}{(1-b_{2\mathrm{R}})}\left(\frac{\ln(\sigma_{\mathrm{c}}-\sigma_{\mathrm{b}})}{\ln(\Delta\varepsilon_{\mathrm{b}})}\right)_{\mathrm{R}}}\approx\frac{\left(\frac{\ln(\sigma_{\mathrm{c}}-\sigma_{\mathrm{b}})}{\ln(\Delta\varepsilon_{\mathrm{b}})}\right)_{\mathrm{N}}}{\left(\frac{\ln(\sigma_{\mathrm{c}}-\sigma_{\mathrm{b}})}{\ln(\Delta\varepsilon_{\mathrm{b}})}\right)_{\mathrm{R}}} \tag{18}$$

where, the subscripts R and N represent the reference and new condition, respectively. n_{hR} and n_{sR} are the parameters at reference condition, and they can be calculated by fitting the reference stress-plastic strain curve. Then n_{hN} and n_{sN} can be calculated by Eqs. 17 and 18. The parameters K_{h} and K_{s} of reference and new conditions can be calculated by Eqs. 4 and 6.

Application, comparisons, and discussion

In this section, the effectiveness of the newly developed model is verified by extensive experiments on IC10.

The reference stress-plastic strain curve is the one measured at the condition of 1173 K, $\dot{\varepsilon}=10^{-4}\mathrm{s}^{-1}$. The parameters ($n_{\mathrm{hR}}$ and n_{sR}) are obtained by fitting the reference curve using Eqs. 1, 4, and 6. The fitted parameters are listed in Table 1.

Figure 4, which shows the comparison of the experimental and the fitted data, illustrates that fitted date fit well with the experiments at reference condition.

Then, the constitutive equations of IC10 follow that

$$\sigma=\begin{cases}\sigma_{\mathrm{cN}}-\dfrac{(\sigma_{\mathrm{cN}}-\sigma_{0.2\mathrm{N}})}{(\Delta\varepsilon_{0.2\mathrm{N}})^{2.96592\left[\left(\ln(\sigma_{\mathrm{c}}-\sigma_{0.2})/\ln(\Delta\varepsilon_{0.2})\right)_{\mathrm{A}}/7.383685\right]}}\left(\varepsilon_{\mathrm{cN}}-\varepsilon_{\mathrm{N}}^{\mathrm{P}}\right)^{2.96592\left[\left(\ln(\sigma_{\mathrm{c}}-\sigma_{0.2})/\ln(\Delta\varepsilon_{0.2})\right)_{\mathrm{N}}/7.383685\right]} & \varepsilon_{\mathrm{N}}^{\mathrm{P}}\le\varepsilon_{\mathrm{cN}}\\ \sigma_{\mathrm{cN}}-\dfrac{(\sigma_{\mathrm{cN}}-\sigma_{\mathrm{bN}})}{(\Delta\varepsilon_{\mathrm{bN}})^{1.52047\left[\left(\ln(\sigma_{\mathrm{c}}-\sigma_{\mathrm{b}})/\ln(\Delta\varepsilon_{\mathrm{b}})\right)_{\mathrm{N}}/2.049042\right]}}\left(\varepsilon_{\mathrm{N}}^{\mathrm{P}}-\varepsilon_{\mathrm{cN}}\right)^{1.52047\left[\left(\ln(\sigma_{\mathrm{c}}-\sigma_{\mathrm{b}})/\ln(\Delta e_{\mathrm{b}})\right)_{\mathrm{N}}/2.049042\right]} & \varepsilon_{\mathrm{N}}^{\mathrm{P}}>\varepsilon_{\mathrm{cN}}\end{cases} \tag{24}$$

Then the equation for a new experimental condition is:

$$\sigma=\sigma_{\mathrm{cN}}-K_{\mathrm{N}}(\Delta\varepsilon)^{n_{\mathrm{N}}}=\begin{cases}\sigma_{\mathrm{cN}}-K_{\mathrm{hN}}(\varepsilon_{\mathrm{cN}}-\varepsilon)^{n_{\mathrm{hN}}} & \varepsilon\le\varepsilon_{\mathrm{cN}}\\ \sigma_{\mathrm{cN}}-K_{\mathrm{sN}}(\varepsilon-\varepsilon_{\mathrm{cN}})^{n_{\mathrm{sN}}} & \varepsilon>\varepsilon_{\mathrm{cN}}\end{cases} \tag{19}$$

where,

$$K_{\mathrm{hN}}=\frac{(\sigma_{\mathrm{c}}-\sigma_{0.2})}{(\Delta\varepsilon_{0.2})^{n_{\mathrm{hN}}}} \tag{20}$$

$$K_{\mathrm{sN}}=\frac{(\sigma_{\mathrm{c}}-\sigma_{\mathrm{b}})}{(\Delta\varepsilon_{\mathrm{b}})^{n_{\mathrm{sN}}}} \tag{21}$$

$$n_{\mathrm{hN}}=\frac{n_{\mathrm{hR}}\left(\frac{\ln(\sigma_{\mathrm{c}}-\sigma_{0.2})}{\ln(\Delta\varepsilon_{0.2})}\right)_{\mathrm{N}}}{\left(\frac{\ln(\sigma_{\mathrm{c}}-\sigma_{0.2})}{\ln(\Delta\varepsilon_{0.2})}\right)_{\mathrm{R}}} \tag{22}$$

$$n_{\mathrm{sN}}=\frac{n_{\mathrm{sR}}\left(\frac{\ln(\sigma_{\mathrm{c}}-\sigma_{\mathrm{b}})}{\ln(\Delta\varepsilon_{\mathrm{b}})}\right)_{\mathrm{N}}}{\left(\frac{\ln(\sigma_{\mathrm{c}}-\sigma_{\mathrm{b}})}{\ln(\Delta\varepsilon_{\mathrm{b}})}\right)_{\mathrm{R}}} \tag{23}$$

As seen in the four equations (Eqs. 20–23), the variation of the parameters K and n at different conditions can be described by the mechanical properties, such as critical stress σ_{c}, yield stress $\sigma_{0.2}$, fracture strength σ_{b}, $\Delta\varepsilon_{0.2}$, and $\Delta\varepsilon_{\mathrm{b}}$.

The values of the mechanical properties which are measured with the tensile experiments are listed in Table 2.

Table 1 Values of the parameters n_{hR} and n_{sR}

Parameters	n_{hR}	n_{sR}
Fitted	2.96592	1.52047

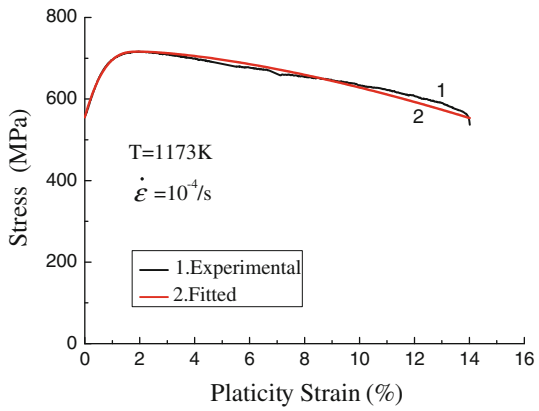

Fig. 4 Comparison of the fitted and experimental curve at $T=1173$ K, $\dot{\varepsilon}=10^{-4}/\mathrm{s}$

Table 2 The values of the mechanical properties (measured by the tensile experiments)

T (K)	$\dot{\varepsilon}$ (s^{-1})	$\sigma_{0.2}$ (MPa)	σ_c (MPa)	ε_c (%)	σ_b (MPa)	ε_b (%)
1173	10^{-2}	849.82	1005.52	1.856	945.83	9.74
1173	10^{-3}	711.66	882.00	2.1	818.19	8.93
1173	10^{-4} (reference state)	555.35	714.63	1.99	566.71	14.01
1273	10^{-2}	499.65	654.12	1.52	411.58	16.75
1273	10^{-3}	395.56	533.26	1.811	419.28	16.64
1273	10^{-4}	292.28	381.19	1.72	239.49	16.59
1373	10^{-2}	286.45	391.00	1.67	157.05	23.99
1373	10^{-3}	210.92	270.98	1.98	182.40	27.62
1373	10^{-4}	150.94	183.21	1.52	125.55	29.42

The constitutive equation for predicting a new curve can be obtained on the basis of the mechanical properties (listed in Table 2) and Eq. 24.

Figure 5 shows the comparisons between the data predicted by the new model and experiments over a wide range of strain rates and temperatures. The predicted data fit well with the experiments, which indicates that the new model is feasible to describe recrystallization behaviors of alloy IC10. The average relative errors $\bar{\delta}$ (see Table 3) at various conditions are less than 3%, which also shows that the new model is effective.

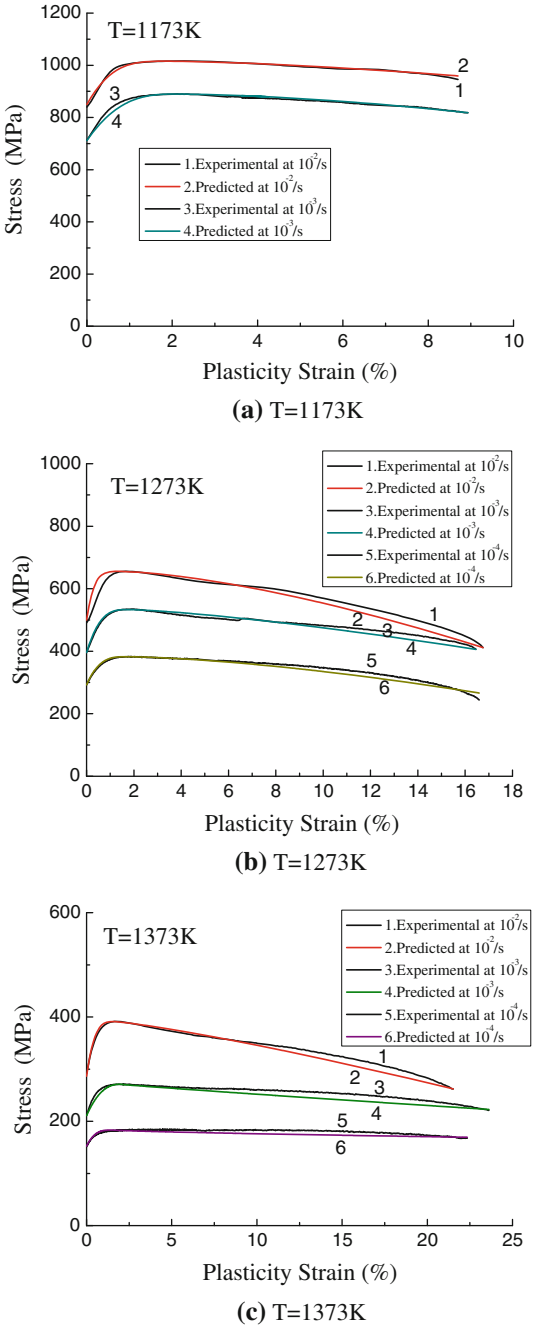

Fig. 5 Comparisons of the stress–strain curves between predicted and experimental of alloy IC10 at different experimental conditions

Summary and conclusions

(1) At the temperature range from 1173 to 1373 K, the domination behavior of IC10 is recrystallization behavior. And the flow stress depends to a high degree on the strain rates and temperatures.

(2) There are both edge and screw dislocations on the cube plane. These dislocations have a tendency to form the slipbands at the interphase boundaries, which is the domination mechanism of recrystallization behaviors.

(3) A new model is developed and used to describe the recrystallization behaviors of alloy IC10. The predicted data fit well with the experiments, and the average relative errors at various conditions are less than 3%. It shows that the model is valid.

Table 3 The average relative errors between predicted data and experimental data (%)

T (K)	1173	1173	1173	1273	1273	1273	1373	1373	1373
$\dot{\varepsilon}$ (s^{-1})	10^{-2}	10^{-3}	10^{-4}	10^{-2}	10^{-3}	10^{-4}	10^{-2}	10^{-3}	10^{-4}
$\bar{\delta}$ (%)	0.35	0.59	0.96	2.79	1.46	1.66	2.01	2.06	2.16

Acknowledgements The financial supports received from the Aviation Science Fund of the People's Republic of China (08B52002) are gratefully acknowledged.

References

1. Han YF, Xing ZP, Chaturvedi MC (1997) In: Nathal MV, Darolia R, Liu CT, Martin PL, Miracle DB, Wagner R, Yamaguchi M (eds) Structural intermetallics. The second international symposium on structural intermetallics, p 713
2. Senba H, Igarashi M (1997) In: Nathal MV, Darolia R, Liu CT, Martin PL, Miracle DB, Wagner R, Yamaguchi M (eds) Structural intermetallics. The second international symposium on structural intermetallics, p 595
3. Lang FQ, Narita T (2007) Intermetallics 15:599
4. Takeuchi S, Kuramoto E (1973) Acta Metall 21(4):415
5. Paidar V, Pope DP, Vitek V (1984) Acta Metall 32(3):435
6. Sun YQ, Hazzledine PM (1988) Philos Mag A 58(4):603
7. Louchet F (1997) Mater Sci Eng A 234–236:275
8. Hirsch PB (1992) Philos Mag A 65(3):569
9. Hirsch PB (1992) Prog Mater Sci 36:63
10. Yin Y (2005) Phd. Sc. thesis, Deptartment of Mechanical Engineering, MIT
11. Cuitiño AM, Ortiz M (1993) Mater Sci Eng A170:111
12. Choi YS, Dimiduk DM, Uchic MD et al (2005) Mater Sci Eng A 400–401:256
13. Choi YS, Dimiduk DM, Uchic MD et al (2006) AFRL-ML-WP-TP 479
14. Zhao XH, Huang ZH, Tan YN et al (2006) J Aeronaut Mater 26(3):20
15. Zhang HJ, Wen WD, Cui HT (2009) Mater Sci Eng A 504:99
16. Zhang HJ, Wen WD, Cui HT et al (2009) Mater Sci Eng A 527:328
17. Zhang HJ, Wen WD, Cui HT, et al (2009) In: TMS 2009 138th Annual meeting & exhibition on proceedings, vol 1: Materials processing and properties, San Francisco, CA, USA, 15–19 Feb 2009, p 219
18. Zhang HJ, Wen WD, Cui HT et al (2008) Acta Aeronaut Astronaut Sin 29(2):499
19. Zhang HJ, Wen WD, Cui HT et al (2009) J Aerosp Power 24(6):1311